Influence of the Physicochemical Properties of Granulated Biofuel on Three-Dimensional Hydrodynamics, Heat Transfer, and Nitrogen Oxide Formation in Small- and Medium-Capacity Hot-Water Boilers

Rachynskyi A.Yu., Baranyuk O.Yu., Tykhokhod V.A., Tkachenko S.S., Pikenin O.A.
National Technical University of Ukraine "Igor Sikorsky Kyiv Polytechnic Institute"
Ukraine, Kyiv

Abstract. The aim of the study is to establish three-dimensional patterns of aerodynamics, heat and mass transfer, particle burnout kinetics, and CO and NO_x emissions in the furnace volumes of 25 and 50 kW hot-water boilers firing six heterogeneous types of fuel pellets using CFD modeling in ANSYS Fluent. To achieve this aim, the following tasks were addressed: 3D polyhedral models of the boiler furnace chambers and gas ducts were developed with detailed representation of burner assemblies and staged air supply; the numerical framework (Euler-Lagrange DPM, Realizable k-ε, DO radiation, diffusion-kinetic char combustion, and detailed NO_x chemistry) was verified against manufacturer data and adiabatic temperatures; velocity, turbulence (*k*), particle burnout, heat-flux (q), and NOx emission fields were investigated when changing from wood to agro-pellets and bottom sludge pellets. The most important results are the demonstration of flame stability (velocity variation ≤ 3.3%) at a fuel burnout degree of 94.0…99.2%, the identification of a 16.1% reduction in peak turbulence with a shift of maximum heat fluxes toward the inclined arch when firing agricultural biomass, the determination of a safe temperature window (1000…1150 °C) against slagging of heating surfaces, and the identification of reducing zones at the flame root (≤ 36 ppm NO_x) suppressing fuel NOx when firing high-nitrogen feedstock ($N^r \leq 3.65\%$). The significance of the results lies in creating a computational and theoretical basis for operating-mode optimization and the safe conversion of serial pellet boilers to low-grade agricultural biomass and organic sludges.

Keywords: hot-water boiler, fuel pellets, agricultural biomass, bottom sludge, CFD modeling, discrete phase model (DPM), polyhedral mesh, heat-flux density, slagging, NO_x emissions.

DOI: https://doi.org/10.52254/1857-0070.2026.4-72.04
UDC: 621.18

Influența proprietăților fizico-chimice ale biocombustibilului granulat asupra hidrodinamicii tridimensionale, transferului de căldură și formării oxizilor de azot în cazanele de apă caldă de capacitate mică și medie

Racinski A.Yu., Baraniuk O.Yu., Tîhokhod V.A., Tkacenko S.S., Pikenin O.A.
Universitatea Tehnică Națională a Ucrainei „Institutul Politehnic Igor Sikorsky din Kiev" Ucraina, Kiev

Rezumat. Scopul studiului este de a determina modelele tridimensionale ale aerodinamicii, transferului de căldură și de masă, cineticii arderii particulelor și formării emisiilor de CO și NO_x în focarele cazanelor de apă caldă cu puteri de 25 și 50 kW, alimentate cu șase tipuri de pelete de combustibil cu proprietăți eterogene, prin utilizarea modelării fluidodinamice computaționale (CFD) în ANSYS Fluent. Pentru atingerea acestui obiectiv, au fost realizate următoarele activități: dezvoltarea unor modele tridimensionale cu elemente poliedrice ale camerelor de ardere și canalelor de gaze ale cazanelor, cu reprezentarea detaliată a ansamblurilor arzătoarelor și a sistemelor de alimentare cu aer în trepte; precum și definirea cadrului de modelare numerică, care include modelul Euler–Lagrange pentru faza discretă (DPM), modelul de turbulență Realizable k–ε, modelul de radiație DO, modelul de ardere a cocsului bazat pe cinetică și difuzie și modelul chimic detaliat al formării oxizilor de azot (NO_x). Cele mai importante rezultate constau în demonstrarea stabilității flăcării, caracterizată printr-o variație a vitezei de cel mult 3.3 %, la un grad de ardere a combustibilului cuprins între 94.0 % și 99.2 %; identificarea unei reduceri cu 16.1 % a intensității maxime a turbulenței, însoțită de deplasarea zonelor cu flux termic maxim către bolta înclinată în cazul utilizării biomasei agricole; determinarea unui interval de temperatură sigur, de 1 000–1 150 °C, pentru prevenirea formării zgurii pe suprafețele de schimb de căldură; și identificarea unor zone reducătoare la baza flăcării, în care concentrația de NO_x este de cel mult 36 ppm, ceea ce inhibă formarea NO_x din azotul conținut în combustibil atunci când se utilizează materii prime cu un conținut ridicat de azot ($N_r \leq 3.65$ %). Semnificația rezultatelor constă în crearea unei baze computaționale și teoretice pentru optimizarea regimurilor de funcționare și pentru conversia în condiții de siguranță a cazanelor pe peleți, proiectate inițial pentru funcționarea în regim standard, în vederea utili zării biomasei agricole de calitate inferioară și a nămolurilor organice.

© Rachynskyi A.Yu., Baranyuk O.Yu., Tykhokhod V.A., Tkachenko S.S., Pikenin O.A. 2026

Cuvinte-cheie: cazan de apă caldă, peleți combustibili, biomasă agricolă, nămol de fund, modelare CFD, model de fază discretă (DPM), rețea poliedrică, densitatea fluxului termic, formarea zgurii, emisii de NOx.

Влияние физико-химических свойств гранулированного биотоплива на трехмерную гидродинамику, теплообмен и образование оксидов азота в водогрейных котлах малой и средней мощности

Рачинский А.Ю., Баранюк А.Ю., Тихоход В.А., Ткаченко С.С., Пикенин А.А.
Национальный технический университет Украины «Киевский политехнический институт имени Игоря Сикорского», Украина, Киев

Аннотация. Целью работы является установление трехмерных закономерностей аэродинамики, тепломассообмена, кинетики выгорания частиц и эмиссии CO и NO_x в топочных объемах водогрейных котлов мощностью 25 и 50 кВт при сжигании шести разнородных видов топливных гранул методами CFD-моделирования в ANSYS Fluent. Для достижения цели решены следующие задачи: построены 3D-полиэдрические модели топочных камер и газоходов котлов с детализацией горелочных узлов и стадийного дутья; верифицирован численный комплекс (Euler-Lagrange DPM, Realizable k-ε, DO-излучение, диффузионно-кинетическое горение кокса, детальная химия NO_x) по паспортным данным и адиабатическим температурам; исследованы поля скоростей, турбулентности (k), степени выгорания частиц, тепловых потоков (q) и эмиссии NO_x при переходе от древесины к агропеллетам и донным илам. Научная новизна результатов заключается в установлении количественной взаимосвязи между свойствами разнородных биотоплив, полиэдрической сеточной топологией и перераспределением локальных тепловых и экологических нагрузок в котлах разной геометрии, а также в доказательстве полного устранения ложной диффузии полиэдрической сеткой в закрученном факеле (T_{core} = 1450…1670 °C, q_{max} до 150 кВт/м^2). Наиболее важными результатами являются доказательство стабильности факела (вариация скорости ≤ 3.3 %) при степени выгорания топлива 94.0…99.2 %, выявление снижения пиковой турбулентности на 16.1 % со смещением максимума тепловых потоков на наклонный свод при сжигании агробиомассы, определение безопасного температурного окна (1000…1150 °C) против шлакования поверхностей нагрева и фиксация восстановительных зон в корне факела (≤ 36 ppm NO_x), подавляющих топливные NO_x при сжигании высокоазотистого сырья (N^r ≤ 3.65 %). Значимость полученных результатов заключается в создании расчетно-теоретического базиса для режимной оптимизации и безопасного перевода серийных пеллетных котлов на низкосортную агробиомассу и органические шламы.

Ключевые слова: водогрейный котел, топливные пеллеты, агробиомасса, донные илы, CFD-моделирование, метод дискретной фазы (DPM), полиэдрическая сетка, плотность теплового потока, шлакование, эмиссия NO_x.

INTRODUCTION

The modern global energy sector is undergoing a profound structural transformation aimed at decarbonizing industry and gradually phasing out conventional hydrocarbon resources. In this context, co-firing biomass with fossil coal in pulverized-coal thermal power plant boilers, as well as in distributed energy systems, is regarded as one of the most economically viable and technologically accessible strategies [1, 2]. As noted in [1], incorporating solid biofuel into the fuel-and-energy balance can not only reduce dependence on non-renewable feedstock but also provide a significant environmental benefit by reducing greenhouse-gas (CO_2), sulfur-oxide, and nitrogen-oxide emissions. At the same time, the technological transition to biomass use involves a number of critical challenges caused by substantial differences in the thermophysical properties of the components: lower heating value of biofuel, accelerated release of volatile matter, changes in the burnout kinetics of the carbonaceous residue, and increased alkali-metal content in the mineral fraction [1, 3, 4].

In conventional thermal-power engineering, thermal calculations and assessments of the operating reliability of furnace chambers are based on standard integral balance methods. However, this approach operates exclusively with average parameters and cannot account for the spatial non-uniformity of radiative-convective heat-transfer processes. Changes in fuel-mixture reactivity led to redistribution of heat-release zones along the furnace height, deformation of the thermal flame core, and local overloading of water-wall tubes [5, 6]. Studies [7, 3, 4] show that the presence of potassium, sodium, chlorine, and sulfur compounds in agricultural-biomass ash promotes the formation of low-melting eutectic phases, sharply increasing the risks of heating-surface slagging, sulfide corrosion, and abrasive erosion of water-wall tubes [7, 8].

Analysis of experimental studies and industrial-test results indicate pronounced staging

and multifactorial behavior in the thermochemical conversion of biofuel:

- Pyrolysis and gas-release kinetics. Study [9] established that agricultural biomass (straw, husks) is characterized by a substantially higher devolatilization rate than wood and coal, which changes the structure of the homogeneous flame and increases the risk of flow segregation in the furnace.
- Emission and thermal-performance indicators. Industrial tests on units of different scales [9, 10, 11] confirmed that partial replacement of coal with plant-based feedstock reduces CO_2 and SO_2 concentrations but makes the boiler's thermal efficiency highly sensitive to the mixing ratio and fuel particle-size distribution [12, 10].
- Mineral residue and circular economy. Studies [13, 8] draw attention to the specific transformation of bottom and fly ash during biomass combustion in fluidized beds, emphasizing the importance of controlling the chemical composition of sludges and ashes.

For an in-depth analysis of the local structure of furnace processes, computational fluid dynamics (CFD) methods are a key tool. Studies [14–16], based on three-dimensional modeling of large-capacity pulverized-coal boilers, have shown that optimizing the biomass injection height and mass fraction can create stable reducing zones in the flame, reducing NO_x generation by 20…50%. The use of integrated numerical approaches for predicting high-temperature corrosion and erosion of boiler tubes [7] confirms the need for precise selection of air-supply operating modes to extend the service life of heating surfaces.

Numerical studies of reaction kinetics and multiphase-flow hydrodynamics based on MP-PIC and CPFD models [17, 18] demonstrate a strong dependence of local temperature fields on flame aerodynamics and oxygen-enrichment conditions. Studies [19] and [7] also demonstrate that staged supply of primary and secondary air is a determining factor in combustion stabilization and minimization of mechanical and chemical incomplete combustion [20, 21]. The specific features and technological limits of implementing co-firing processes for domestic power units were investigated in detail in [2], which substantiated acceptable fuel-substitution ranges for TPP-210A boilers.

For Ukraine's energy sector, diversification of the fuel base and deployment of local renewable energy resources (agricultural-sector waste, biomass, and sludges) are strategic energy-security objectives. This requires a unified computational and theoretical basis for predictive assessment of furnace-equipment performance over a wide range of operating parameters.

The industrial experience of utilizing waste from oil-palm processing (mesocarp fiber, shells, empty fruit bunches, and POME biogas) in power-generation and hot-water boilers is also of considerable scientific and practical interest [23–26]. Research by Z. Effendi and co-authors [23] shows that boiler-unit energy efficiency and fuel-consumption balance depend substantially on feedstock selection (palm varieties), feedwater temperature, and the level of preheating of the combustion air. Studies by M.A. Nasution [24] and S.K. Loh [25] emphasize the large-scale potential of lignocellulosic palm biomass as a strategic renewable resource for cogeneration and distributed-energy systems, where useful energy output per ton of processed feedstock can reach industrial scale while requiring simultaneous control of high-temperature combustion processes. Alongside solid waste, co-firing and direct injection of biogas from palm-oil mill effluent (POME) through modified burner assemblies and forced-draft systems is a promising direction for boiler-fleet modernization, allowing furnace aerodynamics to be optimized and the flame stabilized [26].

Based on the critical analysis of the literature, the authors formulated the objective of the study: to establish fundamental three-dimensional patterns of flow aerodynamics, local heat transfer, thermochemical burnout kinetics of polydisperse particles, and mechanisms of harmful-emission formation (CO, NOx) during direct and co-firing of heterogeneous solid biofuels in the furnace volumes of power and hot-water boilers using comprehensive CFD modeling.

To achieve this objective, the following scientific and practical tasks were addressed:

- Development of spatial geometric and discrete (polyhedral) models of furnace-chamber computational domains with detailed representation of burner assemblies, fuel-supply paths, and staged-air channels.
- Verification of the coupled mathematical framework (RANS k-ε Realizable, Euler-Lagrange DPM, DO radiation, diffusion-kinetic char combustion, and detailed nitrogen-oxide chemistry) against theoretical adiabatic limits and manufacturer thermal-performance data.
- Quantitative analysis of the influence of the component and particle-size composition of

biofuel on the turbulent structure of jets (*k*), velocity fields, and flame-core stability.

- Investigation of the spatial dynamics of solid-phase conversion (Particle Burnout) and localization of radiative-convective heat-flux densities on water-wall surfaces, with identification of slagging and fouling risk zones.
- Identification of nitrogen-containing-compound transformation mechanisms and optimization of the staged aerodynamic supply of oxidizer to minimize total NO_x emissions during thermal utilization of high-nitrogen low-grade feedstock.

METHODS

Spatial modeling of aerodynamics, radiative-convective heat transfer, multistage pellet-burnout kinetics, and NO_x emissions was performed using the finite-volume method in ANSYS Fluent. Interaction between the carrier gas flow and the polydisperse fuel fraction was described using a coupled Euler–Lagrange two-phase approach (Euler-Lagrange DPM, two-way coupling) [27].

The motion of the chemically reacting mixture was described by a steady three-dimensional system of Reynolds-averaged Navier–Stokes (RANS) equations together with continuity, energy, and species-diffusion equations. Turbulence closure was performed using the two-equation Realizable k-ε model with Scalable Wall Functions ($y^+ < 30$), which has demonstrated high accuracy in modeling swirling flame jets [27].

Thermochemical conversion of discrete pellets included heating and moisture evaporation, one-step Arrhenius devolatilization kinetics (A_v = $1{,}0 \cdot 10^5$ s^{-1}, E_v = 88 kJ/mol), and diffusion-kinetic heterogeneous burnout of the char residue (A_c = 0,005 m/(s·K), E_c = 125 kJ/mol) [27]. Combustion of gaseous volatiles was modeled using the Eddy-Dissipation Model, while radiative-energy transport was modeled using the Discrete Ordinates (DO) model with WSGGM absorption and particle shielding effects [27].

NOx formation was calculated in post-processing of the converged hydrodynamic fields, accounting for the Zeldovich thermal mechanism (Thermal NO_x), the fuel-nitrogen destruction mechanism (Fuel NO_x through NH3/HCN intermediates), and heterogeneous reduction on the char surface (Reburning). The complete mathematical description of the differential-equation system, kinetic constants, and mesh-independence verification procedures is presented in the authors' primary study [27].

The following numerical parameters were used in the study:

- Mesh. Unstructured polyhedral meshes adapted in Fluent Meshing with prismatic near-wall layers. Mesh size: $1{,}15 \cdot 10^6$ elements (25 kW boiler) and $1{,}42 \cdot 10^6$ elements (50 kW boiler).
- Pressure–velocity coupling algorithm. Coupled scheme with pseudo-transient relaxation (Pseudo-transient).
- Spatial discretization. Pressure: PRESTO! scheme; momentum, energy, species, turbulence (k, ε), and DO-radiation equations: Second-Order Upwind scheme.
- Convergence criteria: residuals reduced to 10^{-4} for continuity, velocity, k, and ε, and to 10^{-6} for energy, radiation, and NO_x, with stabilization of outlet temperature and O_2, CO_2, and NO concentrations (variation of 0.2% over 200 iterations).

Figure 1 presents the three-dimensional geometric and mesh models of the investigated boiler units, with the boundary conditions for fuel and air supply indicated.

- For the 25 kW SET-25 boiler (Fig. 1a), the computational domain includes a vertical cylindrical retort with screw pellet feed and lower primary-air injection, the furnace chamber, and a tubular heat-exchanger block.
- The 25 kW Kotlant KGP-25 boiler (Fig. 1b) uses a trough-type combustion system with longitudinal screw pellet feeding and distributed lateral air supply through a system of perforated openings, coupled to a three-pass horizontal labyrinth gas duct.
- In the 50 kW Feniks boiler (Fig. 1c), the furnace volume is enlarged and equipped with an inclined radiant arch; the burner assembly provides separate injection of primary air from below and secondary air above the nozzle, as well as additional under-grate air from the ash pit for effective burnout of the polydisperse fraction.

In all models, the water-jacket surfaces were specified as isothermal walls (T_w = 80 °C), while the mesh was locally refined in active-flame zones and near-wall inflation layers were applied along the water-wall surfaces.

The physicochemical, elemental, and thermal-performance characteristics of the investigated biofuels are given in Tables 1–3. Analysis of Tables 1–3 shows that wood pellets have an extremely low content of bound nitrogen (Nr ≤ 0.076%), whereas straw-and-manure agro-pellets and bottom sludges exhibit an unusually high nitrogen concentration (2,78…3,65%). This

confirms the determining role of the Fuel NO_x mechanism (more than 85…90% of total emissions) when firing waste materials.

Analysis of the ballast fraction ($W^r + A^r$, Table 1) shows that the total ballast reaches 26.2% for bottom sludges and 21.1% for straw-and-manure pellets. This explains the prolonged evaporation/heating stage in the DPM model and the reduction of the flame-core temperature peak to 1000…1150 °C compared with wood (>1550 °C).

Analysis of the V^{daf}/FC^{daf} ratio (Table 3) shows that coniferous and mixed wood have the highest volatile-matter yield (75,8…79,2%), resulting in accelerated gas release at the burner nozzle. In contrast, bottom sludges and agro-pellets contain a higher fraction of dense char residue ($FC^{daf} \geq$ 36,4%), requiring a longer particle residence time in the furnace volume to prevent mechanical incomplete combustion.

Table 1.

Physicochemical, elemental, and thermal-performance characteristics of the investigated biofuels

Parameter / Composition	Symbol, unit	Hardwood pellets	Mixed wood of different species	Softwood pellets	Rapeseed pellets	Poultry-manure and straw pellets	Bottom-sludge pellets
Elemental composition on an as-received basis (Ultimate analysis, as-received):							
Carbon	C^r, %	41,568	43,210	46,440	31,560	34,700	30,320
Hydrogen	H^r, %	5,196	5,183	5,850	4,460	4,071	4,060
Oxygen	O^r, %	38,970	39,450	41,590	38,680	25,232	19,850
Nitrogen	N^r, %	0,061	0,044	0,076	0,622	3,653	2,782
Total sulfur	S^r, %	0,026	0,009	0,057	0,064	0,592	0,694
Proximate analysis:							
Moisture, as-received	W^r, %	9,00	0,80	0,40	5,40	13,50	21,80
Ash, as-received	A^r, %	5,18	10,60	5,20	14,90	7,60	4,40
Ash, dry basis	A^d, %	5,69	10,69	5,22	15,75	8,79	5,63
Volatile matter yield	V^{daf}, %	70,0	75,8	79,2	62,5	63,6	59,5
Fixed carbon residue	FC^{daf}, %	30,0	24,2	20,8	37,5	36,4	40,5
Thermal-performance indicators:							
Lower heating value, as-received	Qir, MJ/Kg	14,97	15,67	17,23	10,94	12,93	11,82
Higher heating value (DAF)	Q_s^{daf}, MJ/Kg	18,52	18,74	20,12	17,15	16,84	16,42
Theoretical adiabatic temperature	T_{ad}, °C	1780	1790	1620	1440	1660	1310

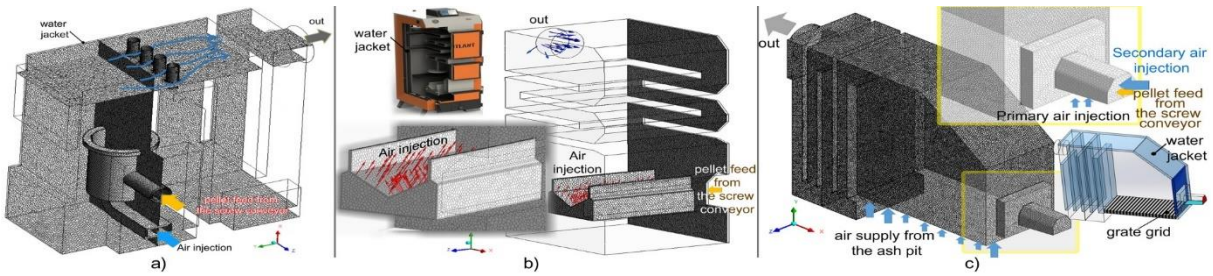


Fig. 1. Spatial computational domains, finite-volume mesh structure, and boundary conditions of the hot-water boilers: a) SET-25 boiler (25 kW) with a vertical retort and tubular heat exchanger; b) Kotlant KGP-25 boiler (25 kW) with a trough-type burner and horizontal labyrinth gas duct; c) Feniks boiler (50 kW) with a flame burner, inclined furnace arch, grate, and developed convective tube bank.

RESULTS AND DISCUSSION

To exclude the influence of spatial discretization on numerical-modeling results and minimize numerical viscosity (false diffusion), a systematic comparison of three mesh topologies was performed: structured hexahedral (Hex), unstructured hybrid (Tetra), and polyhedral (Polyhedral).

Under identical boundary conditions in the swirling burner flame, the hexahedral mesh underestimates the temperature maximum to 500…650 °C because of the non-collinearity between velocity vectors and the coordinate faces of the elements.

A polyhedral mesh with 12…14 adjacent faces provide accurate calculation of spatial gradients of velocity, temperature, and species concentrations in the flame core (peak temperature 1450…1670 °C).

A mesh-convergence study based on the mean-integrated flue-gas temperature for three meshes ($0{,}8\cdot10^6$, $1{,}4\cdot10^6$, and $2{,}2\cdot10^6$ elements) showed that the deviation between the $1{,}4\cdot10^6$ and $2{,}2\cdot10^6$ meshes does not exceed 0.8%.

The numerical model was verified using two independent criteria:

- Manufacturer thermal-performance data: The calculated flue-gas temperature of the 25 kW boiler on the reference fuel was 143 °C versus the manufacturer value of 140 °C (relative error not exceeding 2,1%). For the 50 kW boiler, the outlet temperature was 150…160 °C, corresponding to the specified range of 150…180 °C.
- Thermodynamic limit: Comparison of local peak temperatures from the CFD calculation (t_{max}) with theoretical adiabatic combustion temperatures (Tad), calculated by the standard method, is presented in Table 2.

The aerodynamic structure of the gas flow in the furnace chambers is determined by the interaction of primary air from the burner assembly, secondary tangential air supply, and the geometric configuration of the furnace space.

For the 50 kW boiler with an inclined arch, the calculated velocity fields show preservation of the basic flow topology when the fuel is changed:

- Local velocities in the jet core at the burner-throat outlet lie within the narrow range of 2,31…2,39 m/s (variation not exceeding 3,3%).
- Secondary air forms a recirculation vortex in the upper furnace zone beneath the arch, preventing bypass of unburned gases into the convective shaft.
- At the inlet to the labyrinth channels of the convective tube bank, the velocity profile becomes more uniform, reaching 1,0…1,6 m/s.

For wood pellets with a high volatile-matter yield (V^{daf} = 75,8…79,2%), an extended turbulence zone develops with a maximum k = 0,30…0,31 m²/s², covering the entire flame volume and the jet-turning region.

When switching to high-ash straw-and-manure agro-pellets (A^r = 7,6%, W^r = 13,5%), the peak k value decreases by 16,1% (to 0,26 m²/s²) and shifts directly toward the nozzle exit.

For bottom sludges with a high mineral-ballast content ($W^r + A^r$ = 26,2%), increased flow inertia causes vortex dissipation near the furnace arch ($k \leq 0{,}29$ m²/s²).

Table 2.

Physicochemical, elemental, and thermal-performance characteristics of the investigated biofuels

No.	Fuel type	Q_i^r, MJ/Kg	t_{max} (CFD), °C	T_{ad} (normative method), °C	Relative difference Δt, %
1	Hardwood pellets	14.97	1650	1780	7.3
2	Mixed wood of different species	15.67	1660	1790	7.3
3	Rapeseed pellets	10.94	1280	1440	11.1
4	Softwood pellets	17.23	1450	1620	10.5
5	Poultry-manure and straw pellets	12.93	1430	1660	13.8

No.	Fuel type	Q_i^r, MJ/Kg	t_{max} (CFD), °C	T_{ad} (normative method), °C	Relative difference Δt, %
6	Bottom-sludge pellets	11.82	1140	1310	13.0

Comparison of three-dimensional streamlines and velocity fields (Fig. 2) clearly demonstrates fundamental differences in the hydrodynamic structure of the furnace medium caused by the geometric arrangement of the boiler units.

In the SET-25 boiler (Fig. 2a), air entering through the lower inlet and retort channels forms a vertically directed jet with a maximum local velocity of up to 2.89 m/s at the burner throat. A large symmetrical toroidal recirculation zone with low velocities (0.3…0.7 m/s) forms above the retort, promoting retention of fine particles in the high-temperature volume until they are carried into the vertical convective tube channels.

In the Kotlant KGP-25 boiler (Fig. 2b), the trough-type burner configuration generates counter-directed vortical flows in the lower furnace, intensifying turbulent micromixing of secondary air with pyrolysis products. Upon entering the horizontal three-pass labyrinth gas duct, the flow gradually accelerates around the baffles to 2.5…3.88 m/s, preventing stagnant zones and intensifying convective heat transfer to the water-jacket surfaces.

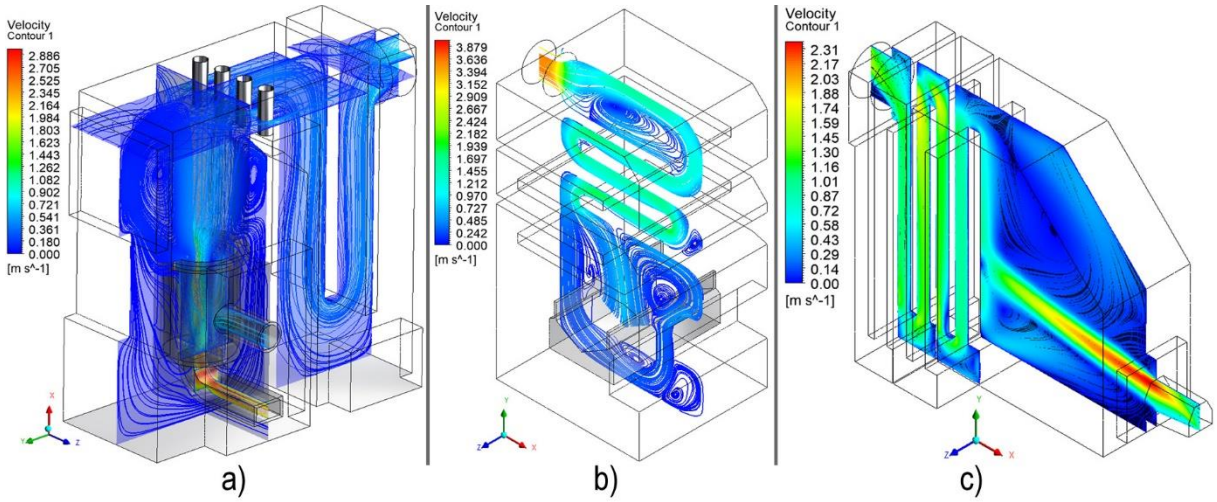


Fig. 2. Spatial streamlines and gas-velocity contours in the computational volumes of the investigated boilers: a) SET-25 (vertical flame jet with near-wall circulation above the retort); b) Kotlant KGP-25 (vortical circulation in the trough-type furnace volume and labyrinth flow in the horizontal channels); c) Feniks (50 kW) (high-velocity inclined flame, interaction with the inclined radiant arch, and a vertical multi-pass downflow/upflow path).

Integration of the equations of motion and thermochemical particle decomposition within the DPM model made it possible to determine the residence time, trajectories, and burnout completeness (Particle Burnout) of pellets along the furnace path:

- Wood pellets (hardwood and coniferous). The high core temperature (>1450 °C) ensures completion of heating and pyrolysis stages within tens of milliseconds. The solid char residue burns out in the flame zone, reaching a burnout degree of 98.5…99.2% before entering the convective section.
- Rapeseed pellets. Due to the release of heavy hydrocarbons and oil components, the active burnout phase is localized 0.1…0.3 m from the burner nozzle, with a burnout degree of 97.0…98,0%.
- Straw-and-poultry-manure pellets. The heterogeneous particle-size distribution causes separation: fine fractions burn out in the swirling flow, while heavy mineralized particles descend into the grate zone, where their burnout is supported by primary air (particle burnout from 96.0% to 97.5%).
- Bottom-sludge pellets. Because of high moisture (21,8%) and low char reactivity,

conversion is extended over the height of the furnace chamber. The burnout degree is 94.0…96.0%, requiring an increased excess-air ratio of primary air to prevent mechanical incomplete combustion.

As a representative example of spatial analysis of discrete-phase burnout, Fig. 5 presents fields of char-residue burnout degree specifically for bottom-sludge pellets. This choice is due to the fact that the investigated bottom sludges have the highest fuel-nitrogen content (N^r = 2.78%), elevated moisture (Wr = 21.8%), and high mineral ballast, making them the most thermochemically inert and critical fuel among the investigated samples. Complete heterogeneous char burnout within the furnace space for such ballast-rich feedstock confirms guaranteed combustion completeness for the other five biofuel types with higher reactivity.

Numerical analysis of the spatial distribution of solid-phase burnout completeness (Particle Burnout) during combustion of bottom-sludge pellets (Fig. 3) confirms the determining influence of the furnace-device aerodynamic configuration on the localization of thermochemical conversion zones of the carbonaceous residue.

In the SET-25 boiler (Fig. 3a), intense thermal decomposition and char burnout (0,70…0,97) are concentrated directly within the cylindrical retort. Fully reacted ash particles are carried into the chamber above the retort, preventing mechanical incomplete combustion in the tubular convective heat exchanger.

In the Kotlant KGP-25 boiler (Fig. 3b), owing to the trough-type topology, the active char-oxidation zone (Burnout → 0.60…0.97) is retained in the bottom layer of the trough, while upward vortical flows ensure burnout of fine fractions in the lower furnace level before they enter the labyrinth channels.

In the 50 kW Feniks boiler (Fig. 3c), high-velocity air-jet supply localizes the primary char-conversion region (Burnout → 0.40…1,0) directly near the burner-nozzle outlet and on the inclined grate. Particles enter the furnace volume after completion of volatile-gasification and with deep burnout of the char residue, ensuring clean convective gas ducts.

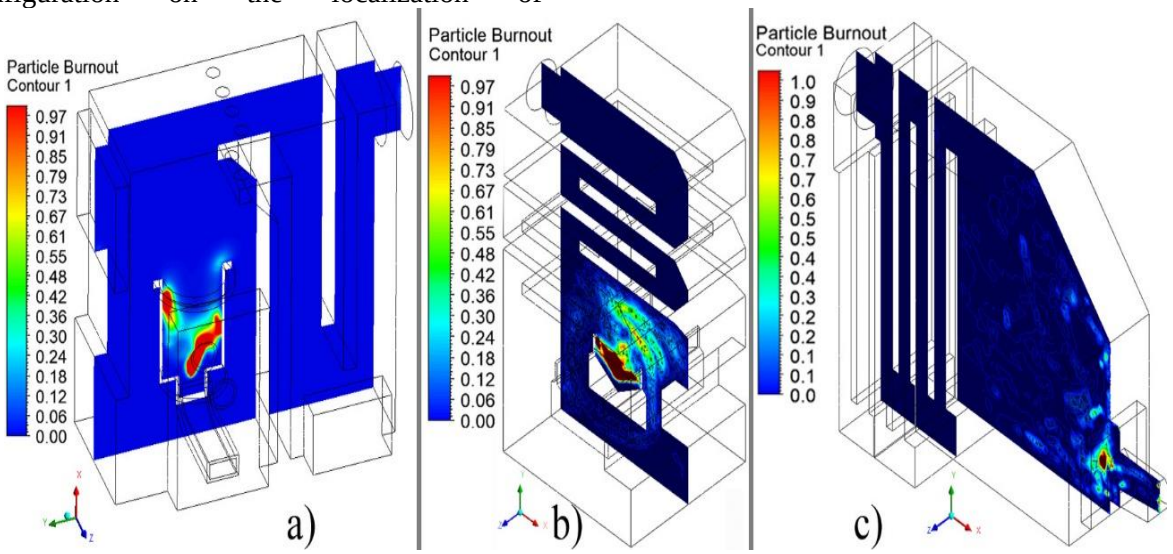


Fig. 3. Spatial fields of char-residue burnout completeness (Particle Burnout, dimensionless fraction) in the computational volumes of the boilers when firing bottom-sludge pellets: a) SET-25; b) Kotlant KGP-25; c) Feniks (50 kW).

Comparison of resultant heat-flux-density fields on the water-jacket surfaces when firing wood pellets (Fig. 4) and bottom-sludge pellets (Fig. 5) reveals a large-scale restructuring of radiative-convective heat removal.

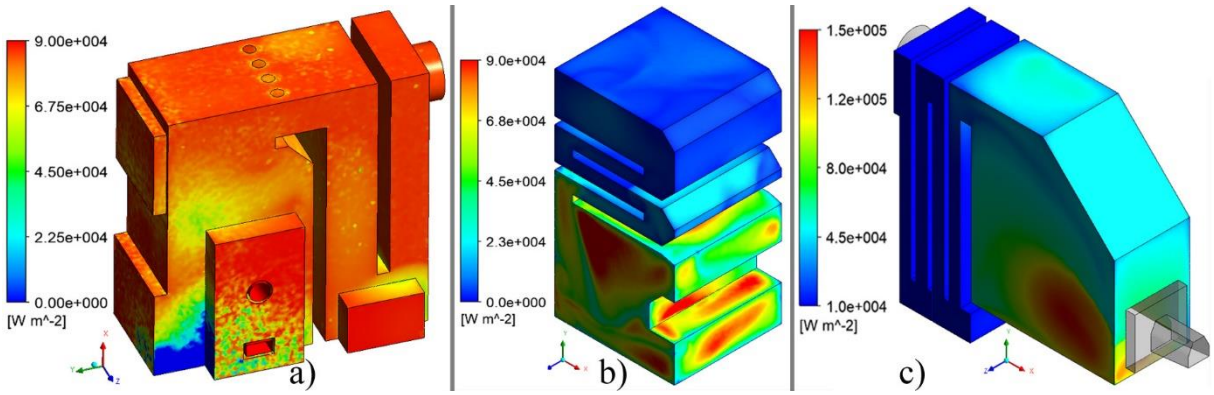


Fig. 4. Spatial distribution of local heat-flux density (q, W/m²) over the heating surfaces of the boiler units when firing hardwood pellets: a) SET-25; b) Kotlant KGP-25; c) Feniks (50 kW).

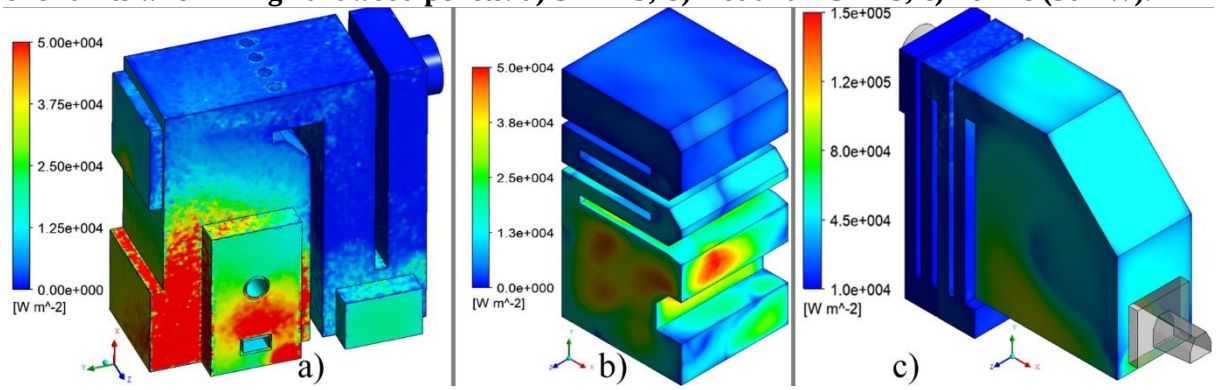


Fig. 5. Spatial distribution of local heat-flux density (q, W/m²) over the heating surfaces of the boiler units when firing low-grade bottom-sludge pellets: a) SET-25; b) Kotlant KGP-25; c) Feniks (50 kW).

SET-25 boiler (Figs. 4a, 5a). When firing high-calorific hardwood, uniformly high heat loading is observed over the entire upper furnace chamber and arch (q = 65…85 kW/m²). When switching to bottom sludges (Fig. 7a), due to the lower flame temperature and gas emissivity, the active heat-absorption zone contracts to the lower retort level (q_{max} ≈ 45…50 kW/m²), while the upper furnace space and tubular block operate under reduced heat removal (q < 15 kW/m²).

Kotlant KGP-25 boiler (Figs. 4b, 5b). For wood fuel, heat fluxes reach a maximum of 80…90 kW/m² on the lower surfaces of the first and second passes of the convective gas duct. When firing ballast-rich sludges, the peak heat-flux density is reduced almost by half (to 35…45 kW/m²) and is concentrated mainly above the trough burner, unloading the subsequent labyrinth channels.

Feniks 50 kW boiler (Figs. 4c, 5c). When firing conditioned wood, the side water-cooled screens exhibit a pronounced thermal-impact zone with an extreme heat-flux density of up to 130…150 kW/m² (dark-red core opposite the flame-expansion zone). When switching to bottom-sludge pellets (Fig. 7c), this high-intensity local zone disappears completely: the heat load on the side screens falls to moderate values of 30…50 kW/m² (green-blue region), eliminating the risks of a local heat-transfer crisis in the near-wall coolant layer and high-temperature metal corrosion.

Comparative analysis of three-dimensional temperature fields for highly reactive wood pellets (Fig. 6) and high-ash bottom-sludge pellets (Fig. 7) reveals fundamental differences in flame thermal structure and temperature filling of the furnace volume:

SET-25 boiler (Figs. 6a, 7a). When firing wood pellets, the active high-temperature combustion core (1450…1650 °C) is localized directly inside the cylindrical retort, with the luminous flame extending into the chamber above the retort. When switching to bottom sludges (Fig. 7a), owing to the significant endothermic effect of moisture evaporation (W^r = 21.8%) and dilution by non-combustible mineral components (A^r = 4.4%), the combustion-core temperature falls to 1050…1140 °C, and the flame height above the retort outlet is substantially reduced.

Kotlant KGP-25 boiler (Figs. 6b, 7b). The trough-type design provides stable maintenance

of localized combustion in the bottom part of the trough. When firing wood, a developed high-temperature flame plume (>650 °C in the lower zone) forms, heating the first heat-exchanger pass. For bottom sludges, the intense heat-release zone is localized strictly within the trough bed, and the gas-cooling gradient in the labyrinth gas duct increases, reducing flue-gas temperature to 98…110 °C.

Feniks 50 kW boiler (Figs. 6c, 7c). The most pronounced scale effect is observed in the 50 kW boiler furnace. When firing hardwood (Fig. 6c), the entire furnace volume is filled with high-temperature gases with 1350…1670 °C isotherms, providing high radiative heat removal to the water-wall surfaces and furnace arch. When switching to bottom sludges (Fig. 7c), the high-temperature region (>1400 °C) is confined exclusively to the initial jet section near the burner nozzle, while the mean chamber temperature decreases to 800…1100 °C (green isotherm region).

This temperature reduction is a positive technological factor when firing low-grade waste because it prevents exceeding the ash deformation and softening onset temperature (T_{soft} ≈ 1150…1200 °C), preventing intensive slagging and adhesion of molten glassy material to the boiler water-wall surfaces. At the same time, effective cooling of flue gases in the multi-pass convective block (to levels <150 °C) confirms preservation of the design heat-production capacity of the heating surfaces.

It should be noted that for the Kotlant KGP-25 (Fig. 6b), the scale is limited to 681.8 °C. This is because the section plane of the Kotlant model passes through the mid-plane of the labyrinth convective gas duct, where the temperature has already decreased after the initial expansion above the trough, or because the selected range represents specifically the gas-duct section.

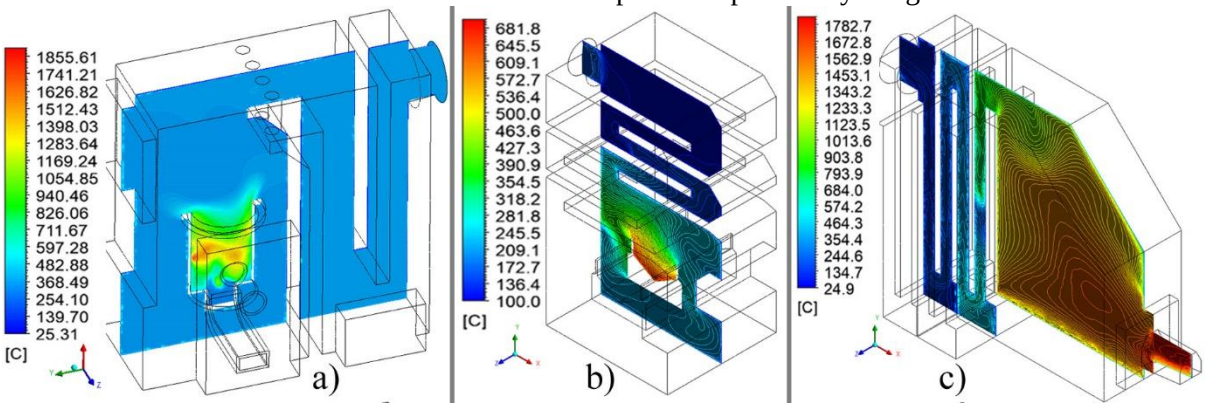


Fig. 6. Spatial temperature fields in the computational volumes of the boilers when firing hardwood pellets (Q_i^r = 14,97 MJ/kg): a) SET-25; b) Kotlant KGP-25; c) Feniks (50 kW).

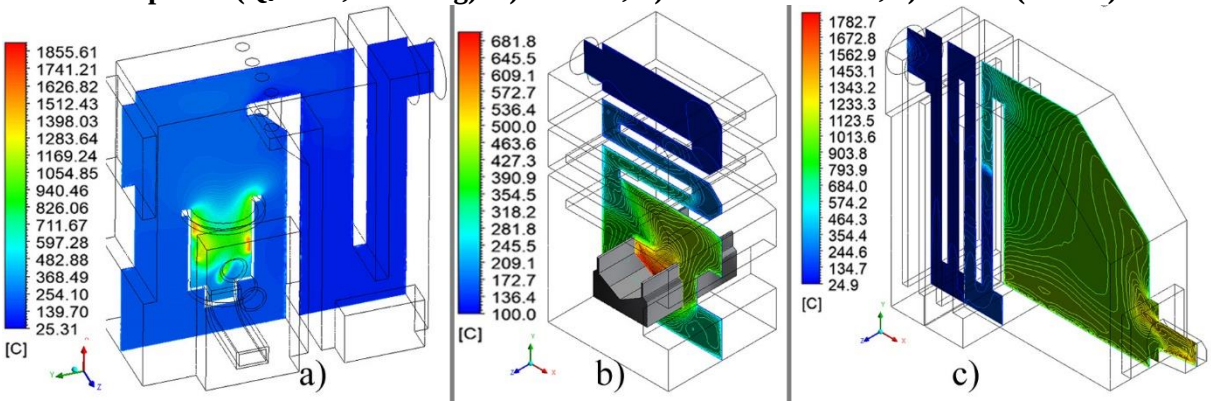


Fig. 7. Spatial temperature fields in the computational volumes of the boilers when firing low-grade bottom-sludge pellets (Q_i^r = 11.82 MJ/kg): a) SET-25; b) Kotlant KGP-25; c) Feniks (50 kW).

Comparative analysis of NO_x concentration fields for bottom-sludge firing (Fig. 8) and conditioned wood pellets (Fig. 9) reveals the dominant role of the fuel mechanism (Fuel NO_x) and the aerodynamic structure of the furnace space.

Generation scale (effect of fuel composition): Switching from conditioned wood to high-nitrogen bottom sludges (N^r = 2,78%) leads to a

multiple increase in peak NO_x concentrations in all three furnace types:

In the SET-25 boiler, the local maximum in the retort increases from 97 ppm to 776 ppm (an 8.0-fold increase);

In the Kotlant KGP-25 boiler, in the trough volume and lower furnace, it increases from 74 ppm to 465 ppm (a 6.3-fold increase);

In the 50 kW Feniks boiler, in the flame core, it increases from 68 ppm to 223 ppm (a 3.3-fold increase).

SET-25 boiler (Figs. 8a, 9a). The active NO_x-formation zone is localized strictly inside the cylindrical retort, where intense volatile release and primary oxidation of nitrogen-containing compounds (HCN/NH_3) occur. However, as the gases leave the retort and enter the chamber above the retort and the convective tube bank, NOx concentration sharply decreases to 48…100 ppm for sludges and to <10 ppm for wood. This is caused by the large recirculation vortex above the retort, where a shortage of free oxygen and the presence of hydrocarbon radicals promote reduction reactions.

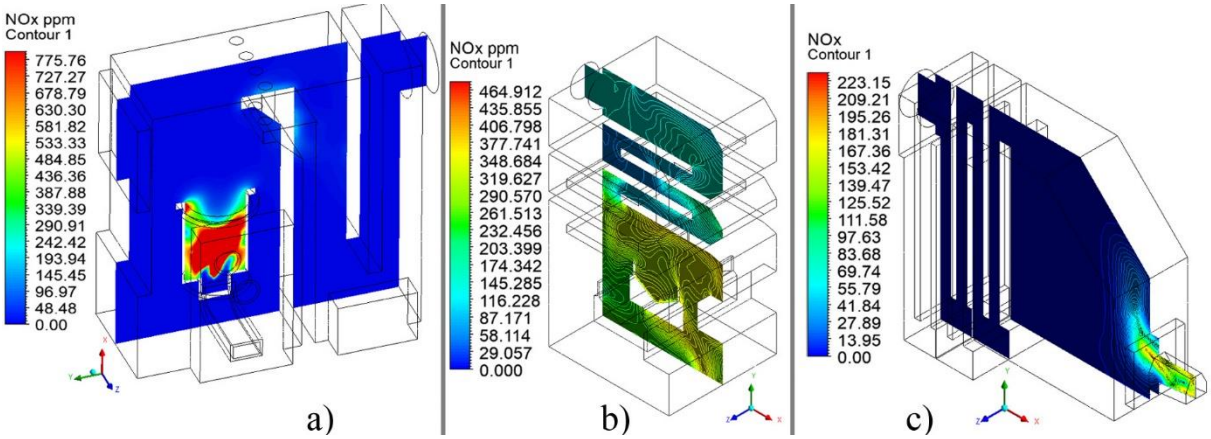


Fig. 8. Spatial distribution of nitrogen-oxide concentration (NO_x, ppm) in the computational volumes of the boiler units when firing high-nitrogen bottom-sludge pellets (N^r = 2.78%): a) SET-25; b) Kotlant KGP-25; c) Feniks (50 kW).

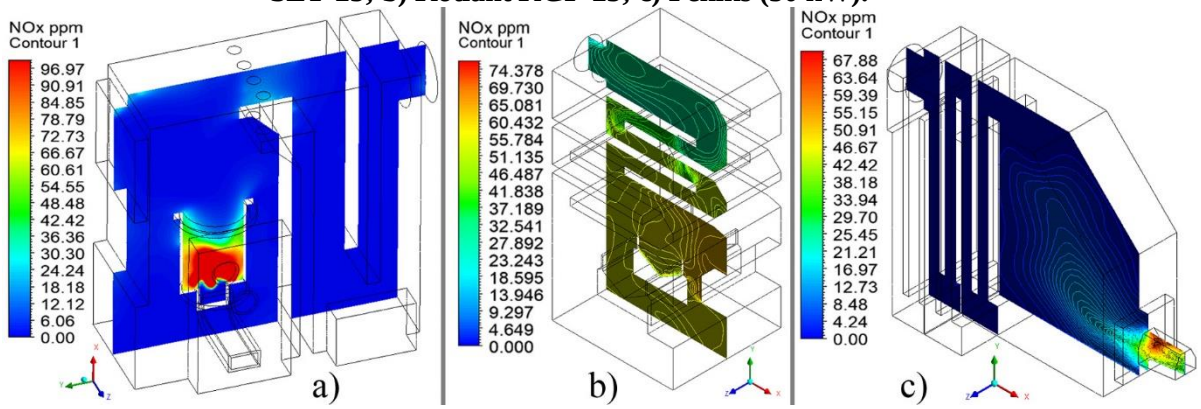


Fig. 9. Spatial distribution of nitrogen-oxide concentration (NO_x, ppm) in the computational volumes of the boiler units when firing low-nitrogen hardwood pellets ($N^r \leq 0.35\%$): a) SET-25; b) Kotlant KGP-25; c) Feniks (50 kW).

Kotlant KGP-25 boiler (Figs. 8b, 9b). In the trough-type furnace chamber, distributed air supply through perforations forms a pronounced zone of moderate NO_x concentrations (230…320 ppm for sludges and 23…37 ppm for wood) filling the entire lower level. As flue gases move through the three-pass horizontal convective labyrinth, the concentration profile becomes more uniform due to turbulent diffusion, and at the boiler outlet the concentration stabilizes at 170…200 ppm (bottom sludges) and 25…30 ppm (wood).

Feniks 50 kW boiler (Figs. 8c, 9c). It demonstrates the strongest NO_x-emission suppression among the investigated units. The high-concentration NO_x zone (150…223 ppm for sludges) is tightly localized exclusively in the initial section of the flame jet near the burner-nozzle outlet. Owing to the large furnace volume, inclined arch, and additional air supply beneath

the grate, an extended oxygen-deficient reducing environment is formed, in which NO_x concentration decreases to 28 ppm already in the middle cross-section of the combustion chamber. At the inlet to the four-pass vertical convective tube bank and at the boiler outlet, NO_x emission levels remain minimal, confirming the high environmental efficiency of volumetric staged combustion.

Analysis of the remaining investigated cases shows that nitrogen-oxide generation has a pronounced spatial character and is controlled by the ratio of the Thermal NO_x and Fuel NO_x mechanisms:

- Suppression zone: In the lower part of the furnace space and at the flame root, a reducing oxygen-free atmosphere with an excess of hydrocarbon radicals forms, where NO_x concentration is minimal (down to 36 ppm). Here, nitrogen oxides are reduced by reactions involving CH_i radicals and the carbonaceous-residue surface ($NO + C(s) \rightarrow 0.5N2 + CO$).
- Effect of nitrogen content N^r: For wood pellets ($N^r \leq 0{,}076\%$), NO_x emission at the boiler outlet is 145…182 ppm (180 ppm for SET-25), which is due to a moderate contribution of the Zeldovich thermal mechanism.
- High-nitrogen feedstock. When switching to straw-and-manure agro-pellets ($N^r = 3.65\%$) and bottom sludges ($N^r = 2.78\%$), oxidation of nitrogen-containing volatiles (NH_3 and HCN) becomes dominant. NO_x concentration in the gas ducts increases to 218…550 ppm.

To keep NOx emissions within environmental limits when firing high-nitrogen agricultural biomass, two-stage air supply with an extended reducing zone in the grate-area space is required.

CONCLUSIONS

Based on the comprehensive study, including three-dimensional numerical CFD modeling of coupled aerodynamics, radiative-convective heat transfer, polydisperse discrete-phase burnout kinetics, and nitrogen-oxide formation in 25 and 50 kW boilers (SET-25, Kotlant KGP-25, Feniks-50) firing six heterogeneous fuel pellets (wood, agricultural biomass, and bottom sludges), the following scientific and practical results were obtained:

1. Fundamental patterns of the spatial aerodynamics of furnace volumes under variation of pellet physicochemical properties were established. It was demonstrated that the structural organization of air supply ensures high hydrodynamic flame stability (local core-velocity variation does not exceed 3,3%) and a high degree of carbonaceous-residue burnout (up to 94,0…99,2%). It was shown that the use of unstructured polyhedral meshes completely eliminates numerical viscosity (false numerical diffusion) in swirling and vortical flows, providing physically adequate reproduction of velocity and turbulent-kinetic-energy gradients.

2. For the first time, the spatial redistribution of local heat fluxes on heating surfaces when switching from conditioned wood to high-ash agricultural-biomass and bottom-sludge pellets was detected and quantitatively characterized. A 16.1% reduction in peak turbulence (to 0.26 m^2/s^2) and a decrease in maximum heat-flux density from 130…150 kW/m^2 to moderate values of 30…50 kW/m^2 were established.

3. A shift of the maximum heat-absorption zone from the side water-wall surfaces to the inclined radiant arch was identified, eliminating the risk of a local near-wall coolant heat-transfer crisis and reducing the intensity of thermofatigue damage to the water-jacket metal.

4. A safe temperature regime of the furnace chambers was substantiated to prevent high-temperature slagging of heating surfaces. It was demonstrated that reducing the mean-volume flame temperature to 1000…1150 °C during thermal utilization of ballast-rich waste (with moisture W^r up to 21.8% and ash content A^r up to 4.4%) keeps gas temperatures below the onset of deformation and melting of low-melting alkali-silicate ash, ensuring stable cleanliness of heat-transfer surfaces without the need to install pulse- or steam-cleaning systems.

5. The mechanism of nitrogen-oxide formation and its spatial transformation during combustion of high-nitrogen biofuels ($N^r \leq 3.65\%$) was revealed. It was demonstrated that, despite increased local Fuel NO_x-generation peaks in the combustion core (up to 776 ppm in the SET-25 retort and 465 ppm in the Kotlant trough), the presence of developed internal recirculation zones and staged air supply forms an oxygen-deficient reducing environment (down to 36 ppm NO_x). This effect is most pronounced in the 50 kW Feniks boiler, where volumetric burnout on the grate suppresses nitrogen oxides directly within the furnace volume, ensuring environmental safety without costly secondary selective non-catalytic reduction systems.

References

[1] Demirbaş A. Potential Applications of Renewable Energy Sources, Biomass Combustion Problems in Boiler Power Systems and Combustion Related Environmental Issues. Progress in Energy and Combustion Science, 2005, vol. 31, no. 2, pp. 171–192. https://www.doi.10.1016/j.pecs.2005.02.002 .

[2] Dzhezhulei V.O., Beztsennyi I.V., Bondzyk D.L., Dunayevska N.I. Technology of Co-firing Coal and Biomass: Features, Current State, and Prospects. Naukovyi Visnyk Natsionalnoho Hirnychoho Universytetu, 2025, no. 4, pp. 46–53. https://www.doi.10.33271/nvngu/2025-4/046 .

[3] Huang H., Gao Y., Hunan C., Wu Y., Wang J., Yu C. et al. Biomass Briquette Fuel, Boiler Types and Pollutant Emissions of Industrial Biomass Boiler: A Review. Particuology, 2022, vol. 77, no. 3, pp. 110–123. https://www.doi.10.1016/j.partic.2022.08.016 .

[4] Mahto K.K., Kumhar R., Thakur R., Mahto O.K., Mandal A., Kumar S., Verma A.K. Industrial Application of Densified Biomass For Heat Generation Systems. International Journal of Creative and Open Research in Engineering and Management, 2026, vol. 2, no. 5, pp. 1–10. https://www.doi.10.55041/ijcope.v2i5.810 .

[5] Cajusol Pingo E.O., Castillo Y., Jiménez Borges R., Zavala de Paz J.P., Castillo Velasquez F.A., Iturralde Carrera L.A., Rodríguez Reséndiz J. Holistic Thermoenergetic Assessment of Biomass Boilers: An Integrated Static, Dynamic, and Energy Framework. Biomass, 2026, vol. 6, no. 3, art. 46. https://www.doi.10.3390/biomass6030046 .

[6] Fajar M., Effendi Z. Analysis of the Effect of Biomass Fuel Feed Rate on the Performance of a 30 Ton h^{-1} Water-tube Boiler in a Palm Oil Mill. RESWARA: Jurnal Riset Ilmu Teknik, 2026, vol. 4, no. 3, pp. 782–790. https://www.doi.10.70716/reswara.v4i3.674 .

[7] Tian Y., Xu X., Zhu L., Zhang L., Wang Q., Li Z. Corrosion and Erosion Risks in Biomass–coal Cofiring Boilers: A CFD-based Safety Assessment of a 660 MW Tangentially Fired Boiler. Energies, 2026, vol. 19, no. 13, art. 3080. https://www.doi.10.3390/en19133080 .

[8] Uliasz-Bocheńczyk A., Pawluk A., Pyzalski M. Characteristics of Ash from the Combustion of Biomass in Fluidized Bed Boilers. Gospodarka Surowcami Mineralnymi – Mineral Resources Management, 2016, vol. 32, no. 3, pp. 149–162. https://www.doi.10.1515/gospo-2016-0029 .

[9] Zhang H., Yu L., Jiang B., Qin C., Jiang S., Yu C. Feasibility Study on Direct Co-firing of Typical Biomass Types in Coal-fired Circulating Fluidized Bed Boilers. Energies, 2026, vol. 19, no. 6, art. 1492. https://www.doi.10.3390/en19061492 .

[10] Mohd Noor N.A.W., Ahmad Sani N.S., Mohd Samsuri M.S.H., Abd.Rahman N., Mohd Ali J., Yusup S. Thermal and Emission Performance of Fuel-based Decarbonization Strategies in Coal-Fired Boilers. SSRN Electronic Journal, 2026. https://www.doi.10.2139/ssrn.6465840 .

[11] Zhang H., Yu C. Experimental Study on Co-firing of Coal and Ciomass in Industrial-scale Circulating Fluidized Bed Boilers. Energies, 2025, vol. 18, no. 14, art. 3832. https://www.doi.10.3390/en18143832 .

[12] Zhang W., Kang D., Xiong Z., Huang Y., Huang S., Zong C., He X. Research on Pollutant Emission Characteristics of Typical Biomass-Fired Boilers. E3S Web of Conferences, 2024, vol. 536, art. 03003. https://www.doi.10.1051/e3sconf/202453603003

[13] Uliasz-Bocheńczyk A., Mokrzycki E. Bottom Ash From Biomass Combustion in Fluidized Bed Boilers in the Context of the Circular Economy. Energies, 2026, vol. 19, no. 3, art. 630. https://www.doi.10.3390/en19030630 .

[14] Fang F., Li Q., Zhang X., Li M., Liu L., Chen W., Liu J. Effect of Biomass Char Injection Position on Combustion and NO Formation in a Tangentially Fired Boiler. Energies, 2026, vol. 19, no. 16, art. 3763. https://www.doi.10.3390/en19163763 .

[15] Du Z., Liu L., Li M., Zhang X., Li Y., Hao M., Ren X. Numerical Simulation of Co-firing Biomass in a 660 MW Coal-fired Boiler. Energies, 2025, vol. 18, no. 23, art. 6082. https://www.doi.10.3390/en18236082 .

[16] Liu L., Li M., Yu D., Ren X. CFD Analysis of Coal and Biomass Co-firing Characteristics in a Tangentially Fired Boiler. Energies, 2026, vol. 19, no. 13, art. 3118. https://www.doi.10.3390/en19133118 .

[17] Liu L., Sun J., Zhang Y.S., Anjum T., Zhang D., Yang J., Ji G. Numerical Investigation of Coal and Rice Husk Co-combustion in an Industrial-Scale Circulating Fluidized Bed: Hydrodynamics, Temperature, and Pollutant Emissions. Processes, 2026, vol. 14, no. 13, art. 2189. https://www.doi.10.3390/pr14132189 .

[18] Pei Y., Wang Y., Zhang X., Li D., Dong N., Ma J., Wang Q. Simulation of Oxygen-enriched Combustion Characteristics of Different Biomass Circulating Fluidized Beds Based on CPFD Model. Processes, 2026, vol. 14, no. 13, art. 2124. https://www.doi.10.3390/pr14132124 .

[19] Silva J., Teixeira S.F.C.F., Teixeira J. Development of a CFD Model to Study the Fundamental Phenomena Associated With Biomass Combustion in a Grate-fired Boiler. Processes, 2025, vol. 13, no. 8, art. 2617. https://www.doi.10.3390/pr13082617 .

[20] Saccani C., Pellegrini M., Guzzini A. Mitigation of Pollutant Emissions from Residential Biomass Boilers. Proc. 13th European Conf. on Industrial Furnaces and Boilers (INFUB-13), Algarve, Portugal, 2022.

[21] Rusovs D., Gromovs S., Meikulans J. Modular Boiler House for Distributed Biomass and RDF Co-incineration. Proc. 25th Int. Sci. Conf. "Engineering for Rural Development", Jelgava, Latvia, 2026. https://www.doi.10.22616/ERDev.2026.25.TF129 .

[22] Zhu J., Lyu Q., Li B., Gao M., Han H. Technology and Application of Preheating Combustion Boilers for Low-carbon Industrial Parks. Chinese Journal of Engineering Science, 2025, vol. 27, no. 5. https://www.doi.10.15302/J-SSCAE-2025.10.001 .

[23] Effendi Z., Aisyah S.N., Hastyanda R. Fuel Used Analysis on Boiler Efficiency Variations and Water Intake Temperature Affected by Palm Oil Varieties. Agro Bali : Agricultural Journal, 2021, vol. 4, no. 1, pp. 94–105. https://www.doi.10.37637/ab.v0i0.634 .

[24] Nasution M.A., Herawan T., Rivani M. Analysis of Palm Biomass as Electricity from Palm Oil Mills in North Sumatera. Energy Procedia, 2014, vol. 47, pp. 166–172. https://www.doi.10.1016/j.egypro.2014.01.210 .

[25] Loh S.K. The potential of the Malaysian Oil Palm Biomass as a Renewable Energy Source. Energy Conversion and Management, 2017, vol. 141, pp. 285–298. https://www.doi.10.1016/j.enconman.2016.08.081 .

[26] Sucahyo B., Hakim D.L., Ridlo R., Puspita T.R., Rosmala E.S. [Kajian Teknologi Pemanfaatan Biogas POME (Palm Oil Mill Effluent) ke Boiler] [Technology Study on the Utilization of POME (Palm Oil Mill Effluent) Biogas to Boilers]. Majalah Ilmiah Pengkajian Industri, 2019 (online 2023), vol. 13, no. 1, pp. 43–54. https://www.doi.10.29122/mipi.v13i1.3219 . (In Indonesian).

[27] Rachynskyi A., Baranyuk O., Chernousenko O., Onysko A., Tkachenko S. Peculiarities of Thermal Regimes and Emission Characteristics of Hot Water Boilers Operating on Heterogeneous Fuel Pellets. Problems of the Regional Energetics, 2026, no. 3, pp. 171–185. https://www.doi.10.52254/1857-0070.2026.3-71.13 .

Information about authors.



Rachynskyi Artur
Associate Professor, Department of Thermal and Alternative Energy Engineering. Research interests: experimental studies of processes in energy equipment. ORCID: 0009-0006-2120-5541 E-mail: arturrachinskiy@gmail.com



Tykhokhod Volodymyr
Associate Professor, Department of Digital Technologies in Energy. Research interests: development of digital twins for energy equipment.ORCID: 0000-0002-1525-4770 E-mail: v.tikhokhod@gmail.com



Pikenin Oleksii
Senior lecturer, Department of space engineering. Research interests: mechanisms, drives, machine components, modeling, design.
ORCID: 0000-0003-2602-4708
E-mail: pikenin.work@gmail.com



Baranyuk Oleksandr,
Associate Professor, Department of Thermal and Alternative Energy Engineering. Research interests: numerical modeling of processes in power equipment. ORCID: 0000-0001-6008-6465 E-mail: AleksandrW@i.ua



Tkachenko Svitlana
Senior lecturer, Department of space engineering. Research interests: mechanisms, drives, machine components, modeling, design, CAD/CAE systems, instrumentation.
ORCID: 0000-0002-6747-5698 E-mail: svittkachenko8@gmail.com